Report

Neuron

# Cortical Circuit Dynamics Are Homeostatically Tuned to Criticality *In Vivo*

## Highlights

- Visual cortical circuits *in vivo* exhibit criticality, an ideal computational regime
- Monocular deprivation disrupts criticality prior to firing rate depression
- Criticality is actively re-established as firing rates are maximally depressed
- Models suggest inhibitory plasticity as a mechanism of a stable computational regime

## Authors

Zhengyu Ma, Gina G. Turrigiano, Ralf Wessel, Keith B. Hengen

## Correspondence

khengen@wustl.edu

## In Brief

Ma et al. evaluate long-term computational dynamics in the visual cortex. Cortical circuits exhibit criticality, a regime that maximizes information processing. Using monocular deprivation, the authors demonstrate that criticality is consistent with a homeostatic set point of emergent dynamics.

Ma et al., 2019, Neuron *104*, 1–10
November 20, 2019 
https://doi.org/10.1016/j.neuron.2019.08.031

CellPress

Please cite this article in press as: Ma et al., Cortical Circuit Dynamics Are Homeostatically Tuned to Criticality *In Vivo*, Neuron (2019), https://doi.org/10.1016/j.neuron.2019.08.031

Neuron
Report



# Cortical Circuit Dynamics Are Homeostatically Tuned to Criticality *In Vivo*

Zhengyu Ma,[1] Gina G. Turrigiano,[2] Ralf Wessel,[1] and Keith B. Hengen[3,4,*]
[1]Department of Physics, Washington University in St. Louis, St. Louis, MO 63130, USA
[2]Department of Biology, Brandeis University, Waltham, MA 02453, USA
[3]Department of Biology, Washington University in St. Louis, St. Louis, MO 63130, USA
[4]Lead Contact
*Correspondence: khengen@wustl.edu
https://doi.org/10.1016/j.neuron.2019.08.031

## SUMMARY

**Homeostatic mechanisms stabilize neuronal activity *in vivo*, but whether this process gives rise to balanced network dynamics is unknown. Here, we continuously monitored the statistics of network spiking in visual cortical circuits in freely behaving rats for 9 days. Under control conditions in light and dark, networks were robustly organized around criticality, a regime that maximizes information capacity and transmission. When input was perturbed by visual deprivation, network criticality was severely disrupted and subsequently restored to criticality over 48 h. Unexpectedly, the recovery of excitatory dynamics preceded homeostatic plasticity of firing rates by >30 h. We utilized model investigations to manipulate firing rate homeostasis in a cell-type-specific manner at the onset of visual deprivation. Our results suggest that criticality in excitatory networks is established by inhibitory plasticity and architecture. These data establish that criticality is consistent with a homeostatic set point for visual cortical dynamics and suggest a key role for homeostatic regulation of inhibition.**

## INTRODUCTION

Neocortical networks give rise to stable activity patterns in the face of perturbation and destabilizing forces; proteins turn over rapidly, Hebbian modifications alter and introduce positive feedback into networks, sensory drive is variable, and environments change over many timescales (Abbott and Nelson, 2000; Kätzel and Miesenböck, 2014; Rasmussen et al., 2017). Homeostatic plasticity mechanisms, which operate via negative feedback, are believed to compensate for these changes and constrain neuronal activity to a firing rate (FR) set point (Turrigiano et al., 1998; Ibata et al., 2008; Tetzlaff et al., 2011; Slomowitz et al., 2015; Hengen et al., 2016). Although these mechanisms are poised to stabilize FRs (Abbott and Nelson, 2000; Turrigiano, 2017), it is unclear whether higher order aspects of neural activity are also subject to active stabilization.

Homeostatic plasticity has been most extensively studied in neocortical pyramidal neurons, which have a variety of cell-autonomous and local microcircuit mechanisms that can counterbalance perturbations in activity (Turrigiano et al., 1998; O'Brien et al., 1998; Turrigiano, 2008; Pozo and Goda, 2010; Lambo and Turrigiano, 2013). Consistent with this, in the visual cortex (V1), long-term visual deprivation initially suppresses neuronal firing (Hengen et al., 2013; Mrsic-Flogel et al., 2007), which then exhibits a homeostatic rebound to baseline levels over multiple days (Hengen et al., 2013; Keck et al., 2013; Barnes et al., 2015). FR rebound is exhibited at the level of individual regular spiking units (RSUs) (presumptive pyramidal neurons; Hengen et al., 2016), congruent with the expression of homeostatic plasticity mechanisms, such as synaptic scaling and plasticity of intrinsic excitability (Ibata et al., 2008; Ancona Esselmann et al., 2017; Lambo and Turrigiano, 2013). In models, similar processes stabilize network output by preventing runaway gain problems caused by synapse-specific plasticity, such as long-term potentiation (LTP) and long-term depression (LTD; von der Malsburg, 1973; Bienenstock et al., 1982; Miller and MacKay, 1994). Although these data suggest a key role for cell-autonomous FR homeostasis in stabilizing brain activity, it is unclear how FR homeostasis contributes to circuit dynamics in the intact brain. Networks *in vivo* are complex and composed of diverse cell types with recurrent and plastic connectivity, and there is evidence that cell-type-specific changes cooperate to influence circuit stability. Inhibitory and excitatory neurons can exhibit opposite and complementary responses to visual manipulation (Maffei et al., 2004), inhibition and excitation must be matched in models of additive recurrent networks to achieve selection and amplification (Wersing et al., 2001), and inhibitory connectivity permits long-term information storage in models of volatile networks (Mongillo et al., 2018). Further, upon sensory deprivation, inhibitory neurons exhibit suppression and homeostatic recovery 24 h prior to excitatory neurons (Hengen et al., 2013; Kuhlman et al., 2013), suggesting a key role for inhibition in direct homeostatic challenges. Ultimately, it is circuit dynamics that must be stabilized, a process that is not an inevitable endpoint of stable neurons (Liberti et al., 2016; Chambers and Rumpel, 2017). What aspects of circuit dynamics serve as a homeostatic endpoint and the underlying mechanisms that stabilize them remain unknown.

Dynamics emerge from the interaction of neurons and establish the computational regime of a network. Cortical networks

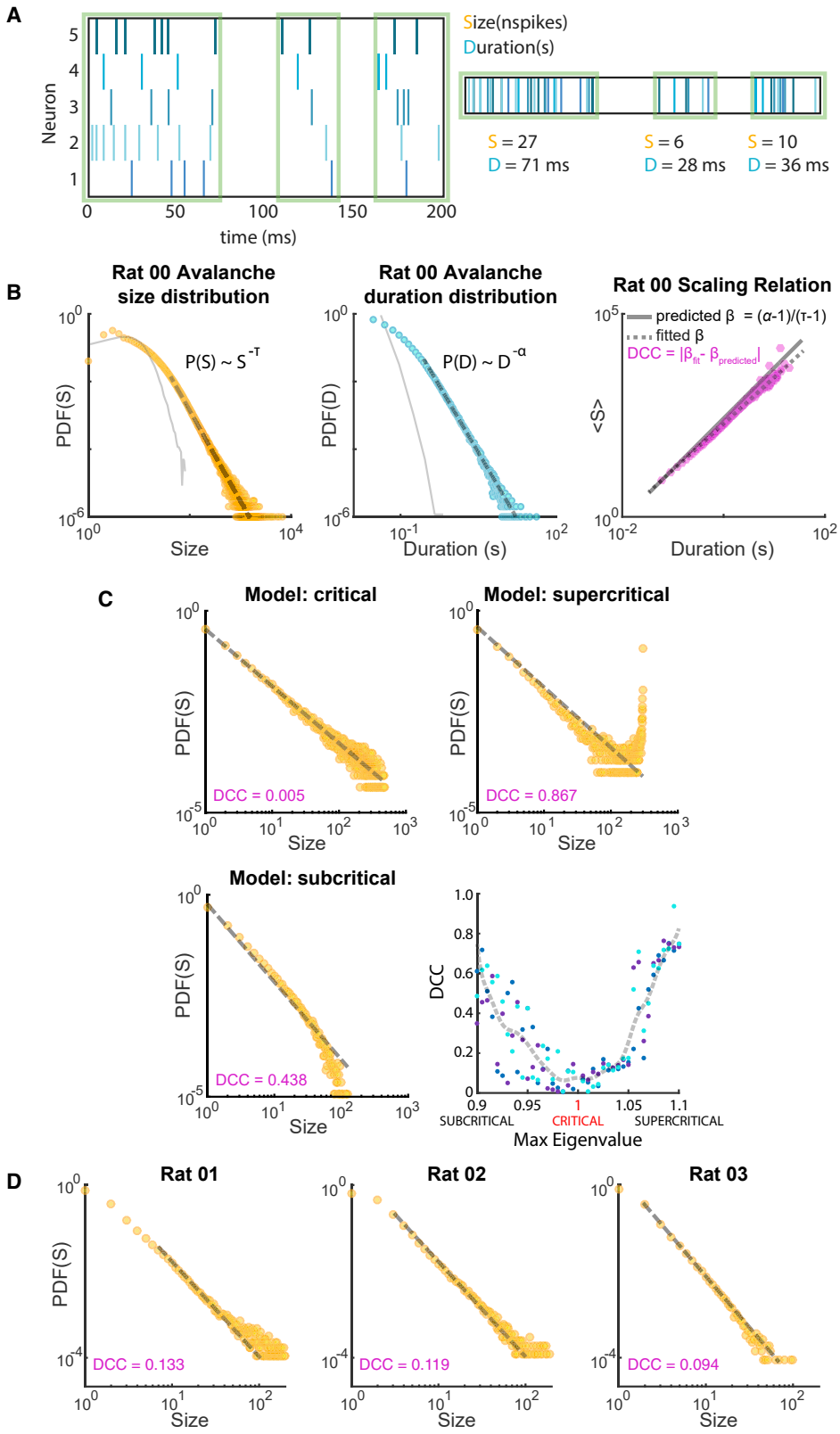


*(legend on next page)*

are assumed to (1) be "balanced," such that runaway gain does not drive the network toward saturation or silence, (2) encode and transmit information across a wide range of spatial (μm to cm) and temporal (ms to min/h/etc.) scales, (3) have a broad dynamic range, and (4) be capable of processing complex information. Each of these criteria falls out of a specific nonequilibrium regime of population dynamics called "criticality," which has been proposed as a possible set point for neuronal networks (Bertschinger and Natschläger, 2004; Priesemann et al., 2014; Shew et al., 2015; Karimipanah et al., 2017). Criticality is a network state poised at the boundary between strongly and weakly coordinated population activity that maximizes information capacity (entropy) and transmission (Shew and Plenz, 2013; Cocchi et al., 2017). Measures of criticality are independent of FR and network size, making it a conceptually attractive candidate for a signature of stable networks capable of normal information processing (Beggs and Plenz, 2004; Haldeman and Beggs, 2005; Beggs, 2008). Previous work suggests that cortical networks are critical (Beggs and Plenz, 2003; Gireesh and Plenz, 2008). Despite this, the possibility that criticality may serve as the set point of homeostatic processes in the intact brain has not been addressed (Shew and Plenz, 2013).

Homeostatic plasticity is difficult to assay in the intact animal, as many compensatory processes serve to counterbalance fluctuations in a wide range of inputs and states. Monocular deprivation (MD) is widely accepted as a direct, physiologically relevant homeostatic challenge to cortical activity *in vivo*. Brief MD (1 or 2 days) results in widespread LTD across V1 and changes the intracortical excitation-inhibition balance (Heynen et al., 2003; Miska et al., 2018), leading to a >50% suppression of neuronal spiking (Hengen et al., 2013, 2016). Prolonged MD reveals homeostatic increases in synaptic strengths and intrinsic excitability (Lambo and Turrigiano, 2013) and a rebound of neuronal activity to baseline levels (Hengen et al., 2016). Recording network spiking continuously in this context allowed us to directly ask whether criticality is also a homeostatic set point of cortical circuits. In this context, we sought to answer three questions: first, to what extent is the cortex "critical" under normal conditions; second, (if cortical activity reflects criticality) is criticality a set point for cortical dynamics; and third, does firing rate homeostasis result in stable network properties?

## RESULTS

To examine whether V1 networks exhibit criticality in freely behaving rats, we combined new recordings with previously collected data, in which we were able to follow extracellular, regular-spiking (RSU) single-unit activity for 168 h from both the deprived and control hemispheres of monocular V1 ($V1_m$) (Hengen et al., 2016) and measured network state with respect to criticality. RSUs (Niell and Stryker, 2008; Hengen et al., 2013) were classified as continuously recorded if spikes within the cluster were present for at least 80% of the 7-day recording period (Hengen et al., 2016; 46 RSUs from 7 animals). Units present for less than 80% of the recordings were classified as non-continuous and considered as individual units within each applicable 4-h bin (MD: 10,280; control: 8,584 RSUs from 7 animals). Network measurements include all single-unit RSUs detectable in each 4-h bin, and measurements of FR homeostasis are based on continuously observable RSUs. All analyses utilize the same 7 animals with simultaneous recordings in control and deprived hemispheres.

Critical systems are defined by scale free dynamics such that events spanning all spatial and temporal scales are observed according to power laws. Events are neither limited to small, local bursts nor do events "snowball" and consume the network. In this context, events are contiguous cascades of spiking activity (Beggs and Plenz, 2003; Gautam et al., 2015) colloquially termed "neuronal avalanches." In other words, avalanches are bursts of spiking activity across a circuit or network, whose start and stop are defined by crossing a threshold of network activity (STAR Methods). Controversially, the observation of power laws in avalanches has been interpreted as an indicator of criticality (see Beggs and Timme, 2012; Wilting and Priesemann, 2018). Power laws are insufficient to indicate criticality and can emerge from noise (Touboul and Destexhe, 2017). The most demanding indicator of criticality is "exponent relation," a measure capable of separating truly critical dynamics from chaos models that generate power laws (Touboul and Destexhe, 2017). To assess exponent relation in our data, avalanches were analyzed in terms of size (S) (the number of spikes) and duration (D) (time; Figures 1A and S1). Power law exponents were fit to the both the size ($\tau$) and duration ($\alpha$) distributions. In critical systems, the relationship between size and duration is described by: $\beta = (\alpha - 1)/(\tau - 1)$. In other words, $\tau$ and $\alpha$ can be used to predict the mean avalanche size ($< S >$) observed at a given duration according to a third power law exponent, $\beta$ (Friedman et al., 2012; Tang and Bak, 1988).

Here, we introduce a quantitative, scalar measure of how close to criticality a system is operating; when $< S >$ is plotted against avalanche duration, the difference between the empirically derived $\beta$ and the predicted $\beta$ serves as a compact measure of the deviation from criticality (deviation from criticality

**Figure 1. DCC, the Deviation from Criticality Coefficient, Is an Effective, Scalar Measure of How Near a Neural Network Is to Criticality**

(A) Discrete relaxation events, i.e., avalanches, are identified in ensemble recordings by the presence of silent periods. Spikes from all neurons in a region of interest can contribute to an avalanche, which is measured as a function of the number of contributing spikes (S) or the event duration (D).

(B) (Left, center) The probability (PDF [probability distribution function]) of observing an avalanche of a given size (gold) or duration (blue) can be fit by power laws, each generating an exponent ($\tau$, $\alpha$); the exponent is the slope of the line in a log-log plot. Solid gray traces display avalanche distributions in shuffled data. (Right) In critical systems, size and duration scale according to the displayed formula. The difference between the predicted exponent (solid gray line) and the observed exponent (dashed gray line) is a quantitative measure of deviation from criticality (deviation from criticality coefficient [DCC]).

(C) Avalanche size PDF and associated DCC extracted from model networks operating in critical (top left), supercritical (top right), and subcritical regimes (bottom left). (Bottom right) Ground truth model testing of DCC is shown. In three model networks (three colors), DCC is compared to the maximum eigenvalue of the adjacency matrix (1.0 indicates a critical regime by definition).

(D) Avalanche size PDFs and DCCs extracted from 4 h of single-unit data in each of three example animals; examples are a subset of the seven animals used for this study. Data in (B) and (D) are derived from control hemisphere ensembles of well-isolated RSUs. Model and empirical data have been fit with power law functions.

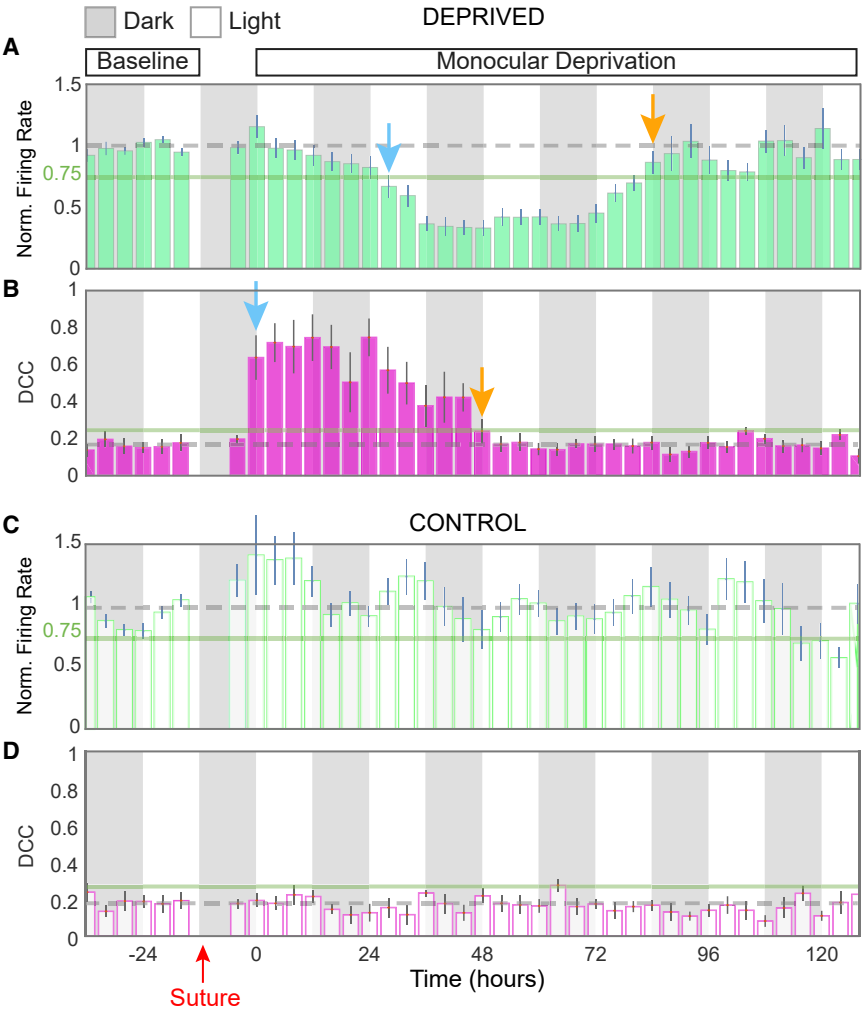


**Figure 2. Network Dynamics Are Homeostatically Tuned to Near-Criticality, Independently of Excitatory FR Homeostasis**

(A) The FRs of continuously observable excitatory neurons followed across 7-day recordings show a biphasic response to monocular deprivation (MD) (47 units; 7 animals). FRs were normalized to 24 h of baseline recordings prior to the induction of MD. FRs were stable for >24 h after the light exposure on the first day of MD (0 h). FRs were maximally suppressed at 36 h (blue arrow) and rebounded to baseline levels by 84 h (gold arrow).

(B) In the same recordings, critical dynamics were assessed. In the first 4 h of light exposure following lid suture, the mean DCC more than tripled (blue arrow). The mean DCC was restored to baseline levels at 48 h (gold arrow).

(C) In the control hemisphere, MD had no significant impact on mean normalized FR of continuously observable units.

(D) Likewise, in the control hemisphere, MD had no significant impact on DCC. Data from the night before MD1 are not shown as they are subject to artifacts from brief anesthesia and lid suture. Dashed gray line is the baseline mean. Solid green line marks 25% change from baseline. Red arrow is time of lid suture. Blue arrow marks the first bin in which data cross the 25% line. Gold arrow marks the first bin in which data return to within 25% of baseline.

Error bars represent SEM.

coefficient ["DCC"]; Figure 1B). This term, DCC, effectively identifies synthetic data tuned to subcritical, critical, and supercritical network states (Figure 1C). In control conditions, *in vivo* cortical circuits were organized close to criticality (DCC < 0.2; Figure 1D).

In addition to DCC, we evaluated network state by employing two additional methods. First, we examined "shape collapse," which tests the necessity that, in critical systems, avalanche profiles of all sizes are revealed to be copies of each other at different scales (Figures S2 and S3; see STAR Methods; Friedman et al., 2012; Ponce-Alvarez et al., 2018). Second, we measured the "branching ratio" or the expected number of neurons activated by one neuron in the previous time step. A network at the critical point will have a branching ratio near 1.0. This approach does not employ the avalanches construct (Figures S2 and S3; see STAR Methods; Wilting and Priesemann, 2018).

## Cortical Circuits *In Vivo* Actively Return to Criticality following Perturbation

The combination of new recordings (n = 2 animals) with earlier datasets (n = 5 animals) further supported previous findings (Hengen et al., 2016). After 28 h of MD, RSU spontaneous single-neuron FR was suppressed by ~60%. By 84 h (the 5$^{th}$ day), the same neurons exhibited a homeostatic rebound to baseline FR (Figure 2A). These results mirror the time course of cellular responses to MD via lid suture (Rittenhouse et al., 1999; Heynen et al., 2003; Lambo and Turrigiano, 2013; Hengen et al., 2013). In stark contrast, cortical circuits deviated from the critical network state rapidly upon light exposure following MD ($DCC \approx 0.6$; Figure 2B) more than 24 h before RSU FRs were perturbed. Cortical circuits returned to near criticality at 48 h while FRs were at the nadir of their suppression. The rapid deviation from criticality at the onset of MD preceded a reduction in pyramidal single-neuron FRs by nearly 30 h (Figures 2A and 2B), similar to the time course of inhibitory FR suppression (Hengen et al., 2013). FR homeostasis of RSUs lagged the resurrection of network criticality by >32 h (Figures 2A and 2B). All animals exhibited this effect (individual animal data in Figures S1 and S4). Control hemisphere FRs and network dynamics were unaffected by MD and showed no significant changes across the time course of the experiments (Figures 2C and 2D). In addition, under baseline conditions (i.e., prior to lid suture), the network state in V1 operated near the critical regime ($DCC \approx 0.2$) in both light and dark (Figure 2B). These data are consistent with the hypothesis that criticality serves as a central attractor of circuit dynamics in V1 of freely behaving animals. The timing of the deviation and subsequent recovery from criticality

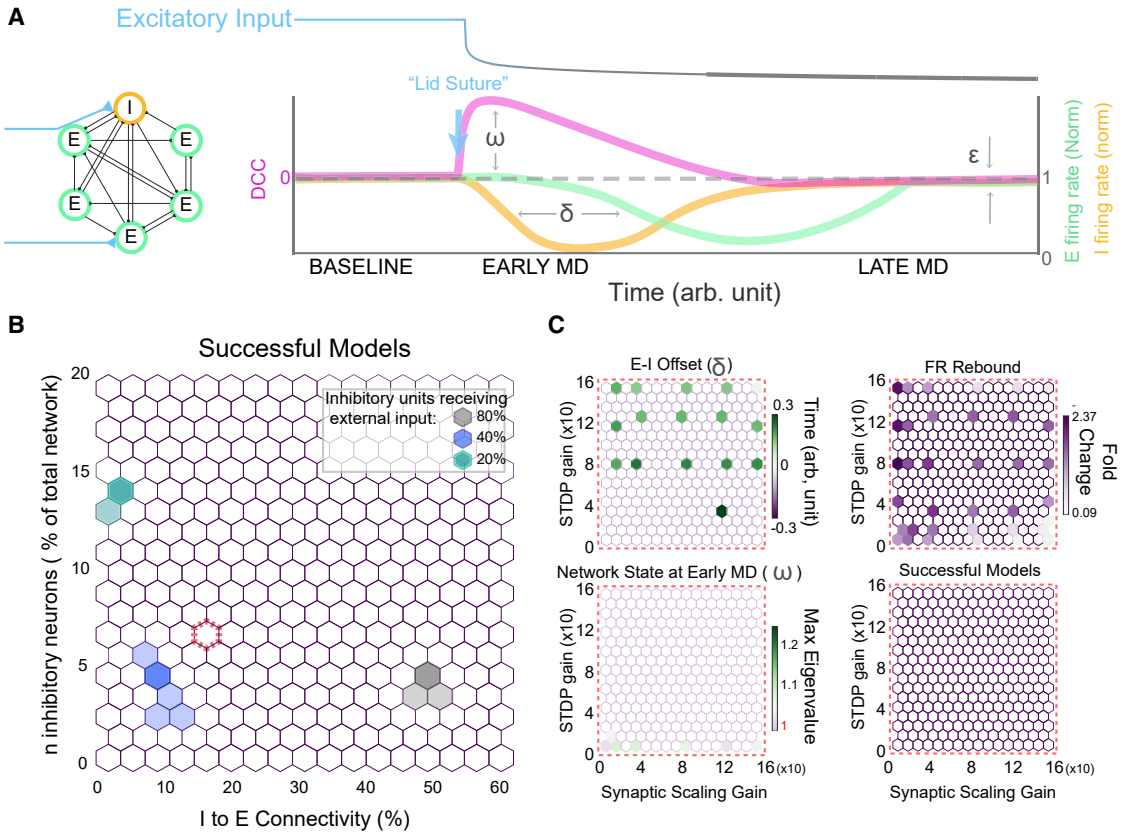


**Figure 3. Inhibitory and Not Excitatory Parameters or Synaptic Plasticity Rules Are Sufficient to Recapitulate Empirical Results in a Series of Models**

(A) (Left) Illustration of model recurrent network with excitatory input (blue) to inhibitory (orange) and excitatory (green) neurons. (Right) Illustration of model time course and "successful" results is shown. Firing rates of excitatory (E) and inhibitory (I) neurons and network state with respect to criticality (DCC) were monitored continuously. In successful models, "lid suture" (reduction in excitatory input, blue/gray line) rapidly increased DCC (ω) and suppressed inhibitory neuron FRs prior to suppressing excitatory neuron FRs (δ), and each of these measures returned to baseline parameters (ε) despite maintained reduction in input.

(B) The inhibitory fraction of the network and the number of excitatory neurons contacted by each inhibitory neuron were systematically varied across three levels of input to inhibitory neurons. Only three discrete combinations of parameters were sufficient to reproduce empirical results (green, blue, and gray).

(C) A reasonable (nearby) but unsuccessful arrangement of inhibitory parameters was selected (dashed red line in B). With these parameters fixed, no explored region in the three-dimensional space defined by homeostatic plasticity gain (synaptic scaling [SS]), spike-timing-dependent plasticity gain (STDP), and excitatory-to-excitatory neuron connectivity (%) was capable of rescuing the model. STDP gain factor was applied to both inhibitory and excitatory terms.

reveals that the organization of the network around this regime cannot be accounted for by excitatory neuron FR homeostasis. The timing of homeostasis around criticality, although measured in excitatory avalanches, is more consistent with the advanced FR drop and rebound of inhibitory neurons (Hengen et al., 2013; Keck et al., 2013).

## Inhibitory Parameters in Network Models Are Essential for Criticality

To understand what aspects of cortical networks might support FR homeostasis and the emergence of an attractor near criticality, we created an abstract model whose key features resembled those found in V1 (Figure 3). Parameters were chosen based on empirically determined values, e.g., inhibitory neurons were the minority of neurons (Markram et al., 2004), and were more broadly connected throughout the network than were excitatory neurons (Packer and Yuste, 2011). Excitatory synapses onto both excitatory and inhibitory neurons expressed homeostatic (synaptic scaling [SS]) and spike-timing-dependent (STDP) (i.e., Hebbian) plasticity mechanisms. SS was a global, multiplicative adjustment of all excitatory synapses onto a neuron that served to compensate for deviations in output. STDP was an activity-dependent increase or decrease in the strength of a specific synapse onto excitatory neurons (Del Papa et al., 2017). To mimic MD, we subjected models to a sustained reduction of excitatory input. In successful models, this manipulation was sufficient to drive an STDP-dependent suppression of activity, similar to that induced by early MD (Hengen et al., 2016). We then searched for subsets of model parameter combinations that replicated our empirical results, specifically (1) a deviation of the network state from criticality upon reduced input; (2) a reduction in FR, first of inhibitory neurons followed by excitatory neurons (Hengen et al., 2013); and (3) a homeostatic recovery of FR and criticality (Figure 3A).

We explored >400 combinations of three parameters: (1) the fraction of inhibitory neurons in the network; (2) the fraction of excitatory neurons contacted by each inhibitory neuron; and (3) the fraction of inhibitory neurons receiving external input. Less than 0.5% of the models satisfied these constraints (Figure 3B). To assess whether non-inhibitory mechanisms were equally effective in reproducing experimental results, we selected inhibitory parameters of a failure regime adjacent to a successful model (Figure 3B, dashed red). With these inhibitory parameters fixed, we varied synaptic plasticity (10- to 150-fold change in gain, SS, and STDP) and excitatory-to-excitatory connectivity (1%–30%). No explored combination was capable of rescuing the results (Figure 3C). Together, these data suggest that real cortical networks have selected for precise excitatory-inhibitory connectivity rules (Yoshimura and Callaway, 2005; Larremore et al., 2011; Tanaka et al., 2012) and that these rules are sufficient to produce critical dynamics.

Our successful models also offered insight into previous empirical findings regarding FR homeostasis. Following MD, excitatory synapses onto both excitatory and inhibitory neurons were acutely subject to synaptic depression (Miska et al., 2018; Kuhlman et al., 2013); the reduced input to excitatory neurons was initially offset by the reduced activity of inhibitory neurons. The initial delay in excitatory FR suppression is thus a result of disinhibition, not a delay in Hebbian LTD. Due to the immediate suppression of inhibitory neuronal activity, homeostatic synaptic plasticity was activated in inhibitory neurons well before excitatory neurons and inhibitory neurons underwent firing rate homeostasis first.

### Inhibitory Homeostatic Plasticity Constrains Network Dynamics

Finally, to probe the contributions of Hebbian and homeostatic synaptic plasticity to FRs and critical dynamics, we re-ran successful models (Figures 4A–4D) and systematically turned off either SS or STDP in either excitatory or inhibitory neurons upon the initiation of input reduction. As expected, the deletion of SS from excitatory neurons resulted in runaway gain that severely destabilized FRs (von der Malsburg, 1973; Abbott and Nelson, 2000; Turrigiano and Nelson, 2004) and the network state with respect to criticality (Figures 4E–4H). Consistent with LTD contributing to the early phase of MD, elimination of STDP from either excitatory or inhibitory neurons prevented the impact of input reduction altogether (Figure S5). In contrast, elimination of SS from inhibitory neurons pushed network dynamics out of the critical regime without causing runaway gain in FRs of either class of neuron (Figures 4I–4L). This reflects the role of broadly connected inhibitory interneurons in establishing a network poised precisely at the transition between decay and saturation.

## DISCUSSION

In this study, we continuously tracked the activity of cortical circuits for 7 days in freely behaving animals. We sought to answer two key questions. First, is criticality consistent with a homeostatic set point for cortical dynamics? Second, if so, are critical dynamics the end result of FR homeostasis? Utilizing MD as a direct homeostatic challenge to neuronal activity in $V1_m$, here we demonstrate that excitatory neural activity in visual cortex is actively organized near criticality, a computationally attractive network regime poised at a phase transition between excitation and inhibition (Shew et al., 2015). This regime is balanced (avoids issues of runaway gain), maximizes information content and transmission in space and time, and maximizes dynamic range. Our data are consistent with previous theoretical suggestions that criticality may function as a homeostatic set point of cortical network dynamics (Shew and Plenz, 2013; Stepp et al., 2015). The disruption and recovery of criticality in excitatory neurons during MD preceded FR changes in the same cells by more than 30 h. This pattern mirrors MD-induced shifts in the FRs of fast-spiking inhibitory interneurons. Our model investigations indicate that homeostatic mechanisms in excitatory neurons are necessary for stable FRs and homeostatic mechanisms in inhibitory neurons establish network interaction magnitude and activity covariance, which directly influence computational regimes, such as criticality. It is important to note that a test of bidirectionality is necessary to fully establish criticality as a homeostatic set point. This requires one of two things: (1) a manipulation opposite that of MD sufficient to drive a sustained increase in V1 activity, e.g., via chronic stimulation of thalamocortical projections, or (2) conditions capable of promoting a supercritical regime independent of FRs, perhaps as the result of intensive learning in a balanced excitation-inhibition network (Bhatia et al., 2019).

Two criticisms have challenged previous work on criticality and emergent network dynamics in general. First, the detection of stable dynamics does not imply active regulation and may reflect an epiphenomenon; despite the self-organization of many neural systems to a common set point, there has been no evidence that these set points are a homeostatically maintained target of network organization (Shew and Plenz, 2013). Second, detection of criticality may be a false positive. Power law distributions can be achieved by independent stochastic surrogates, i.e., disconnected nodes in a complex system (Touboul and Destexhe, 2017). Assays of criticality require extensive sampling, and previous work has been hamstrung by severe subsampling (Ribeiro et al., 2010). Our data offer a uniquely powerful insight into critical dynamics due to the number of avalanche events that we collected in ~200-h recordings. By utilizing an established homeostatic challenge to $V1_m$ (Lambo and Turrigiano, 2013; Barnes et al., 2015), we were able demonstrate that near criticality is eliminated rapidly upon MD and homeostatically resurrected soon thereafter. These changes, which occurred independently of excitatory FRs, cannot be accounted for by stochastic, disconnected systems (Touboul and Destexhe, 2017). Further, that the critical network state in visual cortex spans extended periods of time as well as transitions in light and dark suggests that it is not a result of a subset of initial conditions but a generalized rule.

Our model investigations point to inhibitory interneuron wiring and plasticity in establishing and maintaining criticality in cortical circuits. These findings are consistent with a previous theoretical study that demonstrated a role for inhibitory plasticity in stabilizing networks around criticality (Stepp et al., 2015). Here, the parameters that we imposed upon the model in terms of performance were derived from *in vivo* physiological data. We

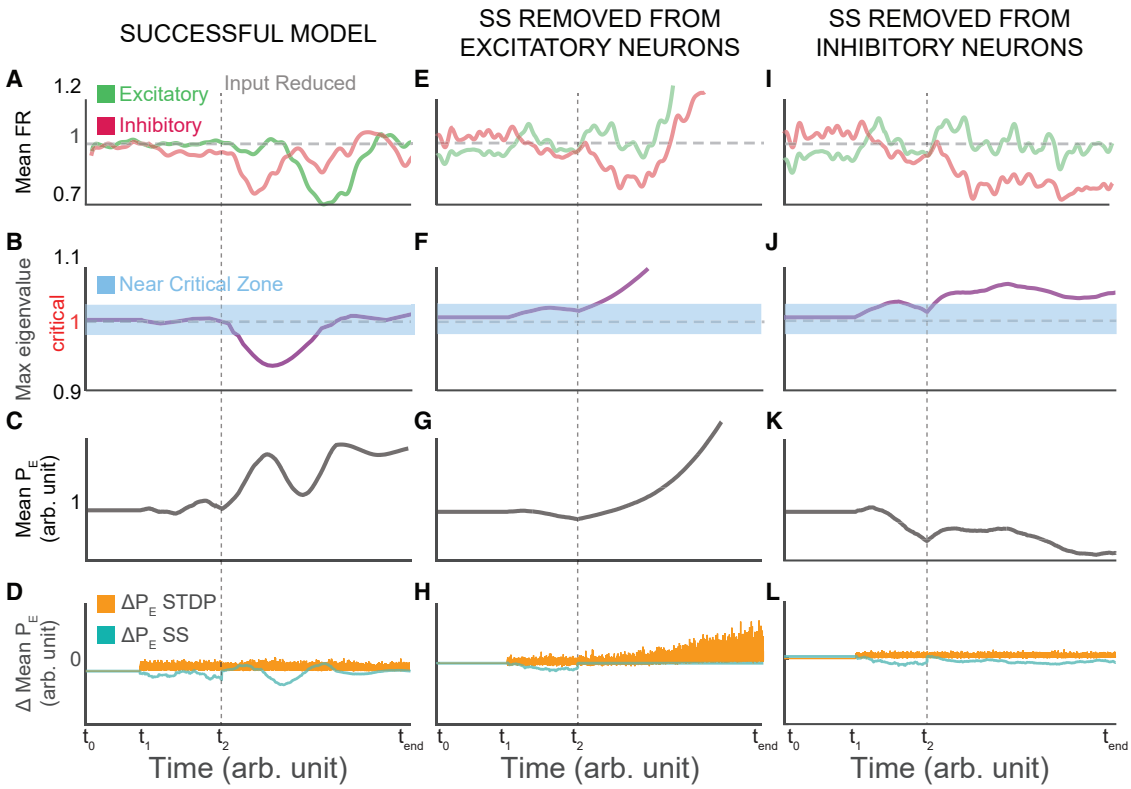


**Figure 4. Excitatory Neuron Homeostatic Plasticity Stabilizes FRs, and Inhibitory Neuron Homeostatic Plasticity Stabilizes Critical Dynamics**

Model cortical networks composed of inhibitory and excitatory neurons were subjected to stable input for 20,000 simulation time steps ($t_0$ to $t_1$). STDP and SS (a global multiplicative compensatory change in synaptic strength) were turned on at 50,000 steps ($t_1$). External input to the network (vertical dashed line, $t_2$) was reduced as a homeostatic challenge mimicking monocular deprivation.

(A–D) Successful models recapitulated empirical results, such that input reduction suppressed FRs of inhibitory neurons (red) prior to excitatory neurons (green) and both rebounded to baseline levels by $t_{end}$ (A) and eliminated the critical network state (max eigenvalue equals 1), which rebounded by $t_{end}$ (B). The mean excitatory synaptic strength (P) across the time course of successful models revealed a net increase by $t_{end}$ (C). The progression of mean P as a function of changes in P due to STDP (orange) and SS (green) is shown (D).

(E–H) Successful models were rerun, and SS was removed from excitatory neurons at the onset of input reduction. Inhibitory and excitatory FRs exhibited runaway gain (E), and network dynamics became unboundedly supercritical (F). Mean P exhibited a similarly unbounded progressive increase (G) as a result of uncompensated STDP (H).

(I–L) Successful models were rerun, and SS was removed from inhibitory neurons at the onset of input reduction. Neither excitatory nor inhibitory FRs exhibited runaway gain (I). Near critical network dynamics were eliminated (J). Mean P exhibited a net reduction (K) and alongside stable SS and STDP (L).

demanded that our model networks be capable of reproducing FR homeostasis. That neurons homeostatically regulate their output is a core prediction of homeostatic synaptic plasticity theory (Turrigiano, 2017) and has been borne out in a variety of preparations (Burrone et al., 2002; Hengen et al., 2013, 2016; Keck et al., 2013), although whether this is true of all neurons and neuronal subtypes is unclear (Barnes et al., 2015). Next, we required that our model respond to input reduction by first decreasing inhibitory FRs and then excitatory FRs. This delay of excitatory suppression relative to both the manipulation and the inhibitory suppression is less well characterized but evident in two prior studies (Hengen et al., 2013; Kuhlman et al., 2013). Assuming that inhibitory interneurons receive significant drive from lateral geniculate nucleus (LGN; Cruikshank et al., 2007; Kloc and Maffei, 2014; Miska et al., 2018) or from pyramidal cells whose primary drive is thalamocortical, this is somewhat predictable; in a heavily recurrent circuit, simultaneously decreasing drive to both inhibitory and excitatory cells logically results in the acute phase of drive reduction being masked (at the level of excitatory cells) via disinhibition. Finally, we required that our model replicate the circuit dynamics with respect to criticality that we describe here (Figure 2). Cortical circuits are robustly critical in our baseline and control hemisphere data, which span a week and include a wide variety of naturally occurring behaviors across light and dark. This measure established a subset of initial conditions for our model as not all topologies are critical (Hellyer et al., 2016). Many sets of parameters were successful when measured against only one constraint (Figure 3); the small set of solutions that overlap across constraints are therefore more likely to provide insight into possible mechanisms *in vivo*.

The addition of the constraints discussed above resulted in a number of notable conclusions. First, in a recurrent network, inhibitory plasticity is insufficient to stabilize criticality, even in systems that start out at criticality. Precisely tuning the

connectivity of inhibitory interneurons to external input and local excitatory neurons was necessary for successful models. Even with inhibitory plasticity intact and criticality at start, models with unsuccessful inhibitory architecture were not rescuable by any tested combinations of homeostatic synaptic plasticity, STDP, and excitatory connectivity (Figure 3). Second, in successful models, we were able to observe the underlying synaptic dynamics (Figures 4A–4D) and test the contribution of cell-autonomous homeostatic synaptic plasticity and STDP in a cell-type-dependent manner. As observed in models decades ago (von der Malsburg, 1973), excitatory neurons with STDP and no homeostatic rule are prone to runaway gain upon synaptic perturbation (Figures 4E–4H). Interestingly, deletion of synaptic scaling from inhibitory cells induced a metaplastic shift in FR set points but did not produce runaway gain. This manipulation, however, eliminated the capacity of networks to reorganize around criticality (Figures 4I–4L). The elimination of STDP in either class of neuron largely prevented the network from responding to input reduction at all (Figure S5). Given the broad connectivity of parvalbumin-positive cortical interneurons (Packer and Yuste, 2011) and previous models that indicate a role for inhibition in stabilizing excitatory patterning (Mongillo et al., 2018), our data suggest that a key role for homeostatic regulation of inhibitory ensembles is to establish and actively maintain the computational regime of excitatory circuitry.

Finally, the relationship between FR homeostasis and criticality is indirect at best. Our data clearly demonstrate that FRs of excitatory neurons need not be stable (within limits) for a network to be critical; criticality dissipates before excitatory FRs have changed, and criticality is re-established when excitatory FRs are maximally depressed. Based on our *in silico* data, it is not difficult to produce a non-critical network with stable activity and similarly a network with drifting FRs and stable, self-organized criticality. Taken in context of recent work, the simplest interpretation of our data is that FR homeostasis of inhibitory interneurons establishes a stable computational regime in which excitatory processing plays out, independent of the total magnitude of spiking activity. It is important that future work test the cell-type-specific roles for inhibitory neurons in long-term network dynamics and examine whether excitatory FR homeostasis is necessary to maintain these regimes on ethologically relevant timescales of learning and experience-dependent plasticity.

## STAR★METHODS

Detailed methods are provided in the online version of this paper and include the following:

- KEY RESOURCES TABLE
- LEAD CONTACT AND MATERIALS AVAILABILITY
- EXPERIMENTAL MODEL AND SUBJECT DETAILS
- METHOD DETAILS
  - *In Vivo* Data Acquisition
  - Data Processing
- QUANTIFICATION AND STATISTICAL ANALYSIS
  - Avalanche Analysis
  - Shape Collapse
  - Branching Ratio
  - Model Investigation
- DATA AND CODE AVAILABILITY

## SUPPLEMENTAL INFORMATION

Supplemental Information can be found online at https://doi.org/10.1016/j.neuron.2019.08.031.

## ACKNOWLEDGMENTS

This work was supported by R00 NS089800 (K.B.H.), R01EY025613 (G.G.T.), NSR35111562 (G.G.T.), Whitehall 20121221 (R.W.), and NSF CRCNS 1308159 (R.W.).

## AUTHOR CONTRIBUTIONS

Conceptualization, K.B.H., R.W., G.G.T., and Z.M.; Methodology, Z.M. and K.B.H.; Software, Z.M.; Formal Analysis, Z.M. and K.B.H.; Investigation, K.B.H. and Z.M.; Resources, K.B.H., G.G.T., and R.W.; Data Curation, K.B.H.; Writing – Original Draft, K.B.H.; Writing – Review & Editing, K.B.H., R.W., G.G.T., and Z.M.; Visualization, K.B.H. and Z.M.

## DECLARATION OF INTERESTS

The authors declare no competing interests.

Received: March 28, 2019
Revised: June 26, 2019
Accepted: August 19, 2019
Published: October 7, 2019

## SUPPORTING CITATIONS

The following reference appears in the Supplemental Information: Fontenele et al. (2019).

## REFERENCES

Abbott, L.F., and Nelson, S.B. (2000). Synaptic plasticity: taming the beast. Nat. Neurosci. *3* (*Suppl*), 1178–1183.

Ancona Esselmann, S.G., Díaz-Alonso, J., Levy, J.M., Bemben, M.A., and Nicoll, R.A. (2017). Synaptic homeostasis requires the membrane-proximal carboxy tail of GluA2. Proc. Natl. Acad. Sci. USA *114*, 13266–13271.

Barnes, S.J., Sammons, R.P., Jacobsen, R.I., Mackie, J., Keller, G.B., and Keck, T. (2015). Subnetwork-specific homeostatic plasticity in mouse visual cortex in vivo. Neuron *86*, 1290–1303.

Beggs, J.M. (2008). The criticality hypothesis: how local cortical networks might optimize information processing. Philos. Trans. A Math. Phys. Eng. Sci. *366*, 329–343.

Beggs, J.M., and Plenz, D. (2003). Neuronal avalanches in neocortical circuits. J. Neurosci. *23*, 11167–11177.

Beggs, J.M., and Plenz, D. (2004). Neuronal avalanches are diverse and precise activity patterns that are stable for many hours in cortical slice cultures. J. Neurosci. *24*, 5216–5229.

Beggs, J.M., and Timme, N. (2012). Being critical of criticality in the brain. Front. Physiol. *3*, 163.

Bertschinger, N., and Natschläger, T. (2004). Real-time computation at the edge of chaos in recurrent neural networks. Neural Comput. *16*, 1413–1436.

Bhatia, A., Moza, S., and Bhalla, U.S. (2019). Precise excitation-inhibition balance controls gain and timing in the hippocampus. eLife *8*, e43415.

Bienenstock, E.L., Cooper, L.N., and Munro, P.W. (1982). Theory for the development of neuron selectivity: orientation specificity and binocular interaction in visual cortex. J. Neurosci. *2*, 32–48.

Burrone, J., O'Byrne, M., and Murthy, V.N. (2002). Multiple forms of synaptic plasticity triggered by selective suppression of activity in individual neurons. Nature *420*, 414–418.

Cardin, J.A., Palmer, L.A., and Contreras, D. (2007). Stimulus feature selectivity in excitatory and inhibitory neurons in primary visual cortex. J. Neurosci. *27*, 10333–10344.

Chambers, A.R., and Rumpel, S. (2017). A stable brain from unstable components: emerging concepts and implications for neural computation. Neuroscience *357*, 172–184.

Clauset, A., Shalizi, C.R., and Newman, M.E.J. (2009). Power-law distributions in empirical data. SIAM Rev. *51*, 661–703.

Cocchi, L., Gollo, L.L., Zalesky, A., and Breakspear, M. (2017). Criticality in the brain: a synthesis of neurobiology, models and cognition. Prog. Neurobiol. *158*, 132–152.

Cruikshank, S.J., Lewis, T.J., and Connors, B.W. (2007). Synaptic basis for intense thalamocortical activation of feedforward inhibitory cells in neocortex. Nat. Neurosci. *10*, 462–468.

Del Papa, B., Priesemann, V., and Triesch, J. (2017). Criticality meets learning: criticality signatures in a self-organizing recurrent neural network. PLoS ONE *12*, e0178683.

Fontenele, A.J., de Vasconcelos, N.A.P., Feliciano, T., Aguiar, L.A.A., Soares-Cunha, C., Coimbra, B., Dalla Porta, L., Ribeiro, S., Rodrigues, A.J., Sousa, N., et al. (2019). Criticality between cortical states. Phys. Rev. Lett. *122*, 208101.

Friedman, N., Ito, S., Brinkman, B.A., Shimono, M., DeVille, R.E., Dahmen, K.A., Beggs, J.M., and Butler, T.C. (2012). Universal critical dynamics in high resolution neuronal avalanche data. Phys. Rev. Lett. *108*, 208102.

Gautam, S.H., Hoang, T.T., McClanahan, K., Grady, S.K., and Shew, W.L. (2015). Maximizing sensory dynamic range by tuning the cortical state to criticality. PLoS Comput. Biol. *11*, e1004576.

Gireesh, E.D., and Plenz, D. (2008). Neuronal avalanches organize as nested theta- and beta/gamma-oscillations during development of cortical layer 2/3. Proc. Natl. Acad. Sci. USA *105*, 7576–7581.

Haldeman, C., and Beggs, J.M. (2005). Critical branching captures activity in living neural networks and maximizes the number of metastable States. Phys. Rev. Lett. *94*, 058101.

Harris, K.D., Henze, D.A., Csicsvari, J., Hirase, H., and Buzsáki, G. (2000). Accuracy of tetrode spike separation as determined by simultaneous intracellular and extracellular measurements. J. Neurophysiol. *84*, 401–414.

Hellyer, P.J., Jachs, B., Clopath, C., and Leech, R. (2016). Local inhibitory plasticity tunes macroscopic brain dynamics and allows the emergence of functional brain networks. Neuroimage. *124*, 85–95.

Hengen, K.B., Lambo, M.E., Van Hooser, S.D., Katz, D.B., and Turrigiano, G.G. (2013). Firing rate homeostasis in visual cortex of freely behaving rodents. Neuron *80*, 335–342.

Hengen, K.B., Torrado Pacheco, A., McGregor, J.N., Van Hooser, S.D., and Turrigiano, G.G. (2016). Neuronal firing rate homeostasis is inhibited by sleep and promoted by wake. Cell *165*, 180–191.

Heynen, A.J., Yoon, B.J., Liu, C.H., Chung, H.J., Huganir, R.L., and Bear, M.F. (2003). Molecular mechanism for loss of visual cortical responsiveness following brief monocular deprivation. Nat. Neurosci. *6*, 854–862.

Ibata, K., Sun, Q., and Turrigiano, G.G. (2008). Rapid synaptic scaling induced by changes in postsynaptic firing. Neuron *57*, 819–826.

Kadir, S.N., Goodman, D.F., and Harris, K.D. (2014). High-dimensional cluster analysis with the masked EM algorithm. Neural Comput. *26*, 2379–2394.

Karimipanah, Y., Ma, Z., Miller, J.K., Yuste, R., and Wessel, R. (2017). Neocortical activity is stimulus- and scale-invariant. PLoS ONE *12*, e0177396.

Kätzel, D., and Miesenböck, G. (2014). Experience-dependent rewiring of specific inhibitory connections in adult neocortex. PLoS Biol. *12*, e1001798.

Keck, T., Keller, G.B., Jacobsen, R.I., Eysel, U.T., Bonhoeffer, T., and Hübener, M. (2013). Synaptic scaling and homeostatic plasticity in the mouse visual cortex in vivo. Neuron *80*, 327–334.

Klaus, A., Yu, S., and Plenz, D. (2011). Statistical analyses support power law distributions found in neuronal avalanches. PLoS ONE *6*, e19779.

Kloc, M., and Maffei, A. (2014). Target-specific properties of thalamocortical synapses onto layer 4 of mouse primary visual cortex. J. Neurosci. *34*, 15455–15465.

Kuhlman, S.J., Olivas, N.D., Tring, E., Ikrar, T., Xu, X., and Trachtenberg, J.T. (2013). A disinhibitory microcircuit initiates critical-period plasticity in the visual cortex. Nature *501*, 543–546.

Lambo, M.E., and Turrigiano, G.G. (2013). Synaptic and intrinsic homeostatic mechanisms cooperate to increase L2/3 pyramidal neuron excitability during a late phase of critical period plasticity. J. Neurosci. *33*, 8810–8819.

Larremore, D.B., Shew, W.L., and Restrepo, J.G. (2011). Predicting criticality and dynamic range in complex networks: effects of topology. Phys. Rev. Lett. *106*, 058101.

Liberti, W.A., 3rd, Markowitz, J.E., Perkins, L.N., Liberti, D.C., Leman, D.P., Guitchounts, G., Velho, T., Kotton, D.N., Lois, C., and Gardner, T.J. (2016). Unstable neurons underlie a stable learned behavior. Nat. Neurosci. *19*, 1665–1671.

Maffei, A., Nelson, S.B., and Turrigiano, G.G. (2004). Selective reconfiguration of layer 4 visual cortical circuitry by visual deprivation. Nat. Neurosci. *7*, 1353–1359.

Markram, H., Toledo-Rodriguez, M., Wang, Y., Gupta, A., Silberberg, G., and Wu, C. (2004). Interneurons of the neocortical inhibitory system. Nat. Rev. Neurosci. *5*, 793–807.

Marshall, N., Timme, N.M., Bennett, N., Ripp, M., Lautzenhiser, E., and Beggs, J.M. (2016). Analysis of power laws, shape collapses, and neural complexity: new techniques and MATLAB support via the NCC Toolbox. Front. Physiol. *7*, 250.

Miller, K.D., and MacKay, D.J.C. (1994). The role of constraints in Hebbian learning. Neural Comput. *6*, 100–126.

Miska, N.J., Richter, L.M., Cary, B.A., Gjorgjieva, J., and Turrigiano, G.G. (2018). Sensory experience inversely regulates feedforward and feedback excitation-inhibition ratio in rodent visual cortex. eLife *7*, e38846.

Mongillo, G., Rumpel, S., and Loewenstein, Y. (2018). Inhibitory connectivity defines the realm of excitatory plasticity. Nat. Neurosci. *21*, 1463–1470.

Mrsic-Flogel, T.D., Hofer, S.B., Ohki, K., Reid, R.C., Bonhoeffer, T., and Hübener, M. (2007). Homeostatic regulation of eye-specific responses in visual cortex during ocular dominance plasticity. Neuron *54*, 961–972.

Niell, C.M., and Stryker, M.P. (2008). Highly selective receptive fields in mouse visual cortex. J. Neurosci. *28*, 7520–7536.

O'Brien, R.J., Kamboj, S., Ehlers, M.D., Rosen, K.R., Fischbach, G.D., and Huganir, R.L. (1998). Activity-dependent modulation of synaptic AMPA receptor accumulation. Neuron *21*, 1067–1078.

Packer, A.M., and Yuste, R. (2011). Dense, unspecific connectivity of neocortical parvalbumin-positive interneurons: a canonical microcircuit for inhibition? J. Neurosci. *31*, 13260–13271.

Poil, S.S., van Ooyen, A., and Linkenkaer-Hansen, K. (2008). Avalanche dynamics of human brain oscillations: relation to critical branching processes and temporal correlations. Hum. Brain Mapp. *29*, 770–777.

Poil, S.S., Hardstone, R., Mansvelder, H.D., and Linkenkaer-Hansen, K. (2012). Critical-state dynamics of avalanches and oscillations jointly emerge from balanced excitation/inhibition in neuronal networks. J. Neurosci. *32*, 9817–9823.

Ponce-Alvarez, A., Jouary, A., Privat, M., Deco, G., and Sumbre, G. (2018). Whole-brain neuronal activity displays crackling noise dynamics. Neuron *100*, 1446–1459.e6.

Pozo, K., and Goda, Y. (2010). Unraveling mechanisms of homeostatic synaptic plasticity. Neuron *66*, 337–351.

Priesemann, V., Wibral, M., Valderrama, M., Pröpper, R., Le Van Quyen, M., Geisel, T., Triesch, J., Nikolić, D., and Munk, M.H. (2014). Spike avalanches in vivo suggest a driven, slightly subcritical brain state. Front. Syst. Neurosci. *8*, 108.

Rasmussen, R.G., Schwartz, A., and Chase, S.M. (2017). Dynamic range adaptation in primary motor cortical populations. eLife *6*, e21409.

Ribeiro, T.L., Copelli, M., Caixeta, F., Belchior, H., Chialvo, D.R., Nicolelis, M.A., and Ribeiro, S. (2010). Spike avalanches exhibit universal dynamics across the sleep-wake cycle. PLoS ONE *5*, e14129.

Rittenhouse, C.D., Shouval, H.Z., Paradiso, M.A., and Bear, M.F. (1999). Monocular deprivation induces homosynaptic long-term depression in visual cortex. Nature *397*, 347–350.

Shew, W.L., and Plenz, D. (2013). The functional benefits of criticality in the cortex. Neuroscientist *19*, 88–100.

Shew, W.L., Clawson, W.P., Pobst, J., Karimipanah, Y., Wright, N.C., and Wessel, R. (2015). Adaptation to sensory input tunes visual cortex to criticality. Nat. Phys. *11*, 659–663.

Slomowitz, E., Styr, B., Vertkin, I., Milshtein-Parush, H., Nelken, I., Slutsky, M., and Slutsky, I. (2015). Interplay between population firing stability and single neuron dynamics in hippocampal networks. eLife *4*, 4.

Stepp, N., Plenz, D., and Srinivasa, N. (2015). Synaptic plasticity enables adaptive self-tuning critical networks. PLoS Comput. Biol. *11*, e1004043.

Tanaka, G., Morino, K., and Aihara, K. (2012). Dynamical robustness in complex networks: the crucial role of low-degree nodes. Sci. Rep. *2*, 232.

Tang, C., and Bak, P. (1988). Critical exponents and scaling relations for self-organized critical phenomena. Phys. Rev. Lett. *60*, 2347–2350.

Tetzlaff, C., Kolodziejski, C., Timme, M., and Wörgötter, F. (2011). Synaptic scaling in combination with many generic plasticity mechanisms stabilizes circuit connectivity. Front. Comput. Neurosci. *5*, 47.

Touboul, J., and Destexhe, A. (2017). Power-law statistics and universal scaling in the absence of criticality. Phys. Rev. E *95*, 012413.

Turrigiano, G.G. (2008). The self-tuning neuron: synaptic scaling of excitatory synapses. Cell *135*, 422–435.

Turrigiano, G.G. (2017). The dialectic of Hebb and homeostasis. Philos. Trans. R. Soc. Lond. B Biol. Sci. *372*, 20160258.

Turrigiano, G.G., Leslie, K.R., Desai, N.S., Rutherford, L.C., and Nelson, S.B. (1998). Activity-dependent scaling of quantal amplitude in neocortical neurons. Nature *391*, 892–896.

Turrigiano, G.G., and Nelson, S.B. (2004). Homeostatic plasticity in the developing nervous system. Nat. Rev. Neurosci. *5*, 97–107.

von der Malsburg, C. (1973). Self-organization of orientation sensitive cells in the striate cortex. Kybernetik *14*, 85–100.

Wersing, H., Beyn, W.J., and Ritter, H. (2001). Dynamical stability conditions for recurrent neural networks with unsaturating piecewise linear transfer functions. Neural Comput. *13*, 1811–1825.

Wilting, J., and Priesemann, V. (2018). Inferring collective dynamical states from widely unobserved systems. Nat. Commun. *9*, 2325.

Yoshimura, Y., and Callaway, E.M. (2005). Fine-scale specificity of cortical networks depends on inhibitory cell type and connectivity. Nat. Neurosci. *8*, 1552–1559.

# STAR★METHODS

## KEY RESOURCES TABLE

| REAGENT or RESOURCE | SOURCE | IDENTIFIER |
|---|---|---|
| Deposited Data | | |
| Dataset and code (python, MATLAB) | This paper | N/A |
| Experimental Models: Organisms/Strains | | |
| Rats, Long Evans | Charles River | Crl:LE |
| Software and Algorithms | | |
| Python > 3.0 | Anaconda | https://www.anaconda.com/distribution/ |
| MATLAB > 2014 | MathWorks | http://www.mathworks.com/ |
| KlustaKwik | Harris et al., 2000 | http://klustakwik.sourceforge.net/ |

## LEAD CONTACT AND MATERIALS AVAILABILITY

Further information and requests for resources should be directed to and will be fulfilled by the Lead Contact, Keith Hengen (khengen@wustl.edu). This study did not generate new unique reagents.

## EXPERIMENTAL MODEL AND SUBJECT DETAILS

We combined two new recordings (see below) with previously published data from five animals (Hengen et al., 2016). All procedures were approved by Brandeis University IACUC and were conducted in accordance NIH guidelines for the use of research animals. Long Evans rats from Charles River were used. Both male and female rats were used, and the rats were postnatal day 21 at the time of electrode implantation (see below).

## METHOD DETAILS

### *In Vivo* Data Acquisition

Experimental design, extracellular recordings, and data collection were as described previously (Hengen et al., 2013, 2016). Briefly, on postnatal day 21 (P21), Long-Evans rat pups of both sexes were anesthetized and a small craniotomy was drilled over monocular primary visual cortex of each hemisphere. Dura was resected and 16ch microelectrode arrays (Tucker-Davis Technologies) were stereotaxically placed with wires spanning all 6 cortical layers. Single wires were implanted bilaterally into the nuchal muscles for electromyographic signal (EMG) acquisition. Animals were allowed to recover from surgery for two days. On the second day of recovery, animals were placed in the environmentally enriched recording chamber (which replicated a home-cage environment) with a litter mate. Continuous data acquisition began after lights-on (ZT0) on P24. Baseline activity was recorded for 24 h (ZT12 of P25 to ZT12 of P26). After lights-out (ZT12) at the end of baseline, animals were briefly disconnected (5-15 minutes) from recording tethers and one eye was sutured. Animals were promptly returned to the recording chamber in complete darkness. Due to the neuronal impact of brief anesthetization, data from the impacted bins of the baseline (P26 dark period) were ignored. The commencement of monocular deprivation (MD) was considered lights-on (ZT0) of P27, at which time animals experienced stimulus-driven ocular disparity for the first time. Recordings were maintained continuously for the next 132h (MD1-MD6). Animal behavior was recorded via synchronized video. All neural data were sampled at 30 kHz and broadband signals were written to disk for offline processing.

### Data Processing

Neural data were bandpass filtered (300 to 10,000 Hz) and thresholded for spike detection (−3.5 SD). Spikes were interpolated, spline fit, and the first four principal components (PCs) of the waveform matrix were calculated. Spike PCs were clustered with Klustakwik (Kadir et al., 2014). Clusters generated by single units were separated from those arising from multiunits with a 15-node random forest trained on > 2,000 single units from previous recordings. The most important feature in single-unit detection was the degree of refractory period contamination. Tested against manually scored datasets, this automated processing generated over 93% agreement. All machine-scored datasets were subsequently manually checked.

Cells were considered continuous if 1) clusters did not drift, 2) single-unit properties were maintained from the beginning of the baseline period until hour 134 (80% of the recording), 3) biophysical properties were consistent with single units (e.g., refractory period, stable waveform), and 4) Signal to noise ratio was high throughout the period considered (> = 80% of the recording). Single

units that were not detectable for at least 80% of the recording were stored separately as transient units. Regular spiking units (RSUs) and fast spiking units were identified based on waveform shape (Niell and Stryker, 2008; Cardin et al., 2007). Only RSUs were considered in this work. The baseline recording (24 h) before lid-suture was used for firing rate normalization of continuous units.

## QUANTIFICATION AND STATISTICAL ANALYSIS

Data are represented as mean ± SD unless otherwise noted. *In vivo* deprived and control hemisphere measurements (DCC and firing rate) were compared with mixed measures ANOVA or multiple comparisons corrected t tests.

### Avalanche Analysis

We discretized time into 40 ms bins, binarized each neuron's spike train into its "activity," i.e., 0 or 1, and obtained the "network activity" as the sum of all recorded activity within the time bin. Based on the network activity, we defined a "neuronal avalanche" by introducing a threshold at the 35$^{th}$ percentile of total network activity (Poil et al., 2008, 2012). Consistent with critical systems, our results were robust across a range of bin sizes (30-500 ms) and thresholds (25 to 45%) For instance, for one 4-h bin of data from baseline from one animal, the DCC ranged from 0.0057 to 0.2358, when choosing all possible combinations of time bin (range 30 to 500 ms) and threshold (range 25 to 45 percentile). For the default choice of 40 ms and 35th percentile, the DCC value was 0.0995 for this example dataset.

An avalanche starts when the network activity crosses the threshold from below and ends when the network activity crosses the threshold from above. We quantified each neuronal avalanche by its size S, i.e., the integrated network activity between threshold crossings, and its duration D, i.e., the time between threshold crossings. Using maximum likelihood estimation methods, we fitted a truncated power law $f(S) = (S^{-\tau} / \sum_{Smin}^{Smax} S^{-\tau})$ to the avalanche size distribution of $N_{av}$ avalanches using the following iterative procedure (Clauset et al., 2009; Klaus et al., 2011). (i) The maximum avalanche size $S_{max}$ was taken as the largest observed avalanche size. (ii) The exponent $\tau$ was estimated for three values of the minimum avalanche size $S_{min}$ ranging from 1 to 10 and the corresponding Kolmogorov-Smirnov (KS) values were obtained. (iii) The minimum avalanche size $S_{min}$ and the corresponding exponent $\tau$ yielding the smallest KS value were chosen. (iv) When $KS < 1/\sqrt{N_{av}}$, the exponent estimation was completed. Otherwise, the procedure (ii) to (iv) was repeated with the maximum avalanche size $S_{max}$ reduced by 1 until the condition $KS < 1/\sqrt{N_{av}}$, was satisfied. We applied the same fitting procedure to the avalanche duration distributions with corresponding exponent $\alpha$. To evaluate whether a power law was a plausible fit of an avalanche distribution, we performed hypothesis testing. We simulated 1000 artificial power law distributions (surrogate distributions) with the same exponent, number of avalanches, minimum avalanche size, and maximum avalanche size, as estimated from the experimental avalanche distribution. Specifically, using the inverse method, the surrogate distributions were generated according to $S = S_{min}(1 - r)^{-1/(\tau-1)}$ where $r$ was a random number drawn from a uniform distribution between 0 and 1. Thereafter, the distribution was upper-truncated by setting a cut-off at the maximum value $S_{max}$ observed in the empirical data. The deviation between the simulated surrogate distributions and a perfect power law was quantified with the KS statistics. The $p$ value was calculated as the fraction of the surrogate distributions with $KS$ values smaller than the $KS$ value of the corresponding experimental avalanche distribution. We took the significance level to be 0.05, i.e., for $p < 0.05$ the power law hypothesis was rejected, whereas for $p \geq 0.05$ the power law hypothesis was not rejected. To test whether average avalanche size scaled with duration according to $<S> \sim D^{\beta}$, we estimated the fitted $\beta$ from the experimental data using linear regression. We then compared the fitted $\beta$ to the predicted $\beta = (\alpha - 1)/(\tau - 1)$. We defined the absolute difference between fitted $\beta$ and predicted $\beta$ as the "Deviation from Criticality Coefficient" (DCC) and adopted this number as a useful measure of the deviation of the network state from criticality.

### Shape Collapse

Friedman et al. (2012) demonstrated that, for a neural system operating at criticality, the size versus duration exponent, $\beta$, can be used to accomplish avalanche shape collapse, where avalanche profiles of different sizes are revealed to be copies of each other at different scales (Figures S2A and S2B). Similarly, this test of criticality was recently performed by Ponce-Alvarez et al., (2018) on the entire zebrafish brain.

When the system is operating near the critical state, avalanches of all durations will reflect the same scaled mean shape. The average number of neurons firing at time $t$ within an avalanche of duration $D$ can be described as $s(t,D) \propto D^{\gamma} F(t/D)$, where $F$ is a universal function determined by $t/D$. Given $\langle S \rangle (D) = \int_0^D s(t,D)dt$, the relationship between $\gamma$ and $\beta$ is $\gamma = \beta - 1$. We utilized the NCC toolbox in MATLAB (Marshall et al., 2016) to perform shape collapse on data from each four-hour bin of data. To be more specific, a scaling exponent $\beta$ was assigned to get $\gamma$, and then $\langle (s(t,D)/D^{\gamma}) \rangle$ was calculated as F(t/D). $\langle\rangle$ denotes the average over avalanches with the same duration. A collection of F(t/D) were extracted for various avalanche durations as F. The average normalized variance of F(t/D) over D is the error for shape collapse under this scaling exponent, as Var(F)/(max(F)-min(F))2. Via this method, a range of scaling exponents $(\beta)$ are tested, and the β that produces the smallest shape collapse is selected as the scaling factor.

Theoretically, the β from shape collapse and the β from the scaling exponent should be the same, despite the fact that they are derived via different methods. At baseline, the mean β from our fitted exponents (scaling relation) was 1.16 and the mean β from shape collapse was 1.08.

To confirm the relationship between critical dynamics and shape collapse, we took advantage of our probabilistic integrate and fire (PIF) model. In the PIF model it is possible to tune the network toward or away from criticality. Specifically, when the maximum eigenvalue (λ) of the network adjacency matrix is precisely 1.0, the network is critical. It is at this point that e.g., the dynamic range of a network is maximized (Larremore et al., 2011). We mapped the relationship between λ and shape collapse error (Figures S3A and S3B). We modeled networks with 2000 neurons and $6x10^5$ time steps with a range of $\lambda$ from 0.81 to 1.14. We utilized the shape collapse NCC tool box (Marshall et al., 2016).

While the shape collapse is a noisier metric than DCC (Figure 1C), error is minimized in critical regimes (Figure S3B). Avalanches were grouped in 40 ms bins; for shape collapse, avalanches with durations from 3 to 100 bins (120 to 4,000 ms) were considered. Beyond 100 bins, there were not enough avalanches to conduct meaningful shape collapses across the time course of our recordings, largely due to the effects of early monocular deprivation (i.e., when DCC was greatest). This is consistent with previous work (Marshall et al., 2016). It is worth noting that the NCC toolbox requires gaps of silence to define avalanches. In model datasets, tuning network λ to > 1 (supercritical) results ceaseless activity. To define avalanches for shape collapse modeling, we thresholded network activity as described above (Avalanche Analyses).

## Branching Ratio

Based on the work of Wilting and Priesemann (2018) we examined the branching ratio of the networks sampled in our recordings. Summarily, the branching ratio is the ratio of the number of neurons spiking at time n+1 to the number of spiking neurons at time n. Critical regimes, by their nature, are balanced and avoid runaway gain (positive or negative) and have a branching ratio of 1.0 (Figure S2C). The methods introduced by Wilting and Priesemann (2018) are robust to severe subsampling and thus provide an effective alternative approach to assessing critical dynamics in our recordings.

In a network with $A$ active neurons at time $t$, if the branching ratio is a fixed value then $<A_{t+1}|A_t> = mA_t + h$ where $<|>$ denotes the conditional expectation, $m$ is the branching ratio and $h$ is a mean rate of an external drive/stimulus. Considering subsampling, $a_t$ is proportional to $A_t$ on average $<a_t|A_t> = \eta A_t + \xi$, where $\eta$ and $\xi$ are constants. This subsampling lead to a bias: $m(\eta^2 Var[A\,t]\,/Var[a\,t\,] - 1)$. Instead of using time $t$ and $t+1$, this method focuses on times $t$ and $t+k$ with different time lags $k = 1,\ldots,k_{maximum}$. With this, the branching ratio $m_k$ is $<a_{t+k}|a_t> = m_k = \eta^2 Var[A_t]/Var[a_t] m^k = bm^k$, where b is a constant. To compute $m_k$ with different $k$, we obtained an exponential curve and extracted $m$ from this curve. For details see Wilting and Priesemann (2018).

We examined a range of $k$ and searched different results using $k_{maximum}$ from tens to one thousand. We then chose $k_{maximum}$ for each animal by checking the baseline period. We selected $k_{maximum}$ as the $k$ that returned $m$ closest to 1.0 during baseline. For the seven animals used in this study, $k_{maximum}$ values were selected for each animal during the recording baseline and maintained throughout the remainder of the experiment.

Consistent with our results based on DCC, the branching ratio was stable near 1.0 at baseline and transiently dropped at the onset of monocular deprivation (Figure S2D).

## Model Investigation

We simulated a model network consisting of 4750 excitatory and 250 inhibitory binary probabilistic model neurons with sparse connectivity and external inputs. Connectivity between excitatory neurons and from excitatory to inhibitory neurons was 3%. Connectivity from inhibitory to excitatory neurons was varied between 1 and 60%. The strength of the connection from neuron $j$ to neuron $i$ is quantified in terms of the transition probability $P_{ij}$, which is the probability that a spike in neuron $j$ causes a spike in neuron $i$ in the next simulation time step (Karimipanah et al., 2017). In order to allow for inhibitory connections, $P_{ij}$ was allowed to be negative for these connections. The binary state $X_i(t)$ of neuron $i$ denotes whether the model neuron spikes $(X_i(t) = 1)$ or does not spike $(X_i(t) = 0)$ at time $t$. At each time step, the state of all neurons was updated synchronously according to the following update rule:

$$X_i(t+1) = \Theta\left[(1-\eta_i(t))\sum_j P_{ij}X_j(t) + \eta_i(t) - \xi_i(t)\right]$$

where $\xi_i(t)$ is a random number in $[0\ 1]$ drawn from a uniform distribution, and $\Theta$ is the step function. The external input $\eta_i(t)$ quantifies the probability of that neuron spiking due to the external input alone. External input was added to 10 percent of the excitatory neurons and a variable percentage (20, 40, and 80%) of the inhibitory neurons. The external input was chosen to be smaller than the transition probability $P_{ij}$, which itself was small for large networks, $P_{ij} \sim 1/N$, where $N$ is the total number of neurons in the network. Because of the weak external inputs, we can employ the approximation $1 - \eta_i \approx 1$ in the above update rule. The external input $\eta_i(t)$ was modeled as a binary Poisson process followed by smoothing with a Gaussian filter with a width of 20 time steps. The maximum eigenvalue $\lambda$ of the transition probability matrix $P_{ij}$ describes the network state: $\lambda < 1$ denotes subcritical regime, $\lambda \approx 1$ denotes the near critical regime and $\lambda > 1$ denotes the supercritical regime (Karimipanah et al., 2017). Here, $\lambda = 1.02$ corresponded to networks operating at the critical regime. Because of the sparse connectivity, most transition probability matrix elements are zero. For the existing connections, the $P_{ij}$

values were drawn from a uniform distribution and then scaled by a constant factor to reach the desired maximum eigenvalue $\lambda$. By default, $P_{ij}$ was constant in the first part of the simulation.

After the first 20,000 time steps, two forms of synaptic dynamics were permitted. Spike-timing dependent plasticity (STDP) was added according to:

$$\delta P_{ij}^{EE}(t) = K_{STDP}\left[X_i^E(t)X_j^E(t-1) - X_j^E(t)X_i^E(t-1)\right]$$

$$\delta P_{ij}^{EI}(t) = -K_{inh}X_j^I(t-1)\left[1 - X_i^E(t)(1+\frac{1}{\mu_I})\right]$$

where $\delta P_{ij}^{EE}(t)$ is the change of connection strength from excitatory neuron to excitatory neuron while $\delta P_{ij}^{EI}$ is the change of connection strength from inhibitory neuron to excitatory neuron induced by STDP and $\mu_I$ is the mean firing rate of all I neurons during baseline (Del Papa et al., 2017). The parameter $K_{STDP}$and $K_{inh}$ is a constant gain value. Synaptic scaling (SS) was added to both E and I cells according to $\delta P_{ij}^{SS}(t) = K_{SS}[F_i^{ref} - F_i^{hist}(t)]$, where $\delta P_{ij}^{SS}(t)$ is the change in synaptic strength according to SS and the parameter $F_i^{ref}$ is the reference firing rate for each single neuron, which provides a set point of firing rate, and $F_i^{hist}(t)$ is the weighted firing rate across a 15,000 step time window. In other words, SS was a global, multiplicative change in all of the synaptic inputs onto a neuron that functioned to compensate for alterations in the neuron's output. SS in excitatory neurons affected both excitatory and inhibitory inputs, while SS in inhibitory neurons affected only inhibitory to inhibitory connections. We found that firing rate and network dynamics are relatively stable in the presence of STDP and SS. To mimic a homeostatic challenge in the model, we reduced the external input $\eta_i(t)$ in an exponential manner leveling out at half the starting value.

Models that satisfied the following constraints were considered successful: 1) the firing rates of both excitatory and inhibitory neurons dropped below a threshold of 75% of normalized baseline activity, 2) the absolute value of the difference of the maximum eigenvalue of the transition probability matrix and 1.02 was larger than 0.05 before the dropping of the excitatory neuron firing rate, i.e., the network became non-critical prior to the disruption of excitatory neuronal firing rate. This corresponds to a DCC of > 0.2. At the end of the experiment, the sum of the excitatory and inhibitory neuron firing rate difference from baseline firing rate was less than 0.09. i.e., firing rates rebounded to baseline levels. Likewise, at the end of the experiment, the maximum eigenvalue returned to a near-critical zone (i.e., within 0.05 of 1.02, defined *a priori* as criticality in this context). This corresponds to a DCC to a value of < 0.2.

## DATA AND CODE AVAILABILITY

The datasets/code supporting the current study have not been deposited in a public repository because of ongoing work, but they are available from the Lead Contact on request (khengen@wustl.edu).